33rd EPS Conference on Plasma Phys. Rome, 19 - 23 June 2006 ECA Vol.**30I**, P-2.128 (2006)

Fluctuation Measurements in the SOL of ASDEX Upgrade by Langmuir Probes

P. Balan,[a] V. Naulin,[c] J.J. Rasmussen,[c] A. Kendl,[a] C. Ionita,[a] R. Schrittwieser,[a]
A. Herrmann,[b] M. Maraschek,[b] H.W. Müller,[b] V. Rohde,[b] ASDEX Upgrade Team[b]

[a]*Association EURATOM-ÖAW, Inst. for Ion Physics and Applied Physics, LFU Innsbruck, Austria,*

[b]*Association EURATOM-IPP Garching, ASDEX Upgrade Group, Garching, Germany*

[c]*Association EURATOM-Risø National Laboratory, OPL-128, Risø, Roskilde, Denmark*

1. Introduction

The underlying mechanisms of the generation of $E\times B$ sheared flows and parallel flows play an important role in the access to improved confinement regimes in magnetically confined toroidal plasmas. One source for sheared poloidal flow is electrostatic turbulence which can drive flows via divergences in the turbulent transport of poloidal momentum, measured by the Reynolds stress. Except for its role for flow generation, the relation between Reynolds stress and the fluctuation-induced particle flux is not well documented. To address these questions measurements of density, potential and temperature, as well as their fluctuations, were performed in the edge plasma region of ASDEX Upgrade.

2. Experimental set-up

A fast reciprocating probe shaft on the ASDEX Upgrade midplane manipulator was used, on which a probe head with five carbon fibre composite pins (each with 1 mm diameter and 2 mm length) was mounted (see Fig. 1). Three pins (*ul* – upper left, *ll* – lower left and *m* – middle) measure the floating potential V_{fl}. The poloidal spacing between probes *ul* and *ll* is 5 mm. Probe *m* is radially protruding by 5 mm from the plane of the other probes. Assuming the electron temperature to be equal on all three probe positions, the radial and poloidal electric field components $E_{r,\vartheta}$ are obtained from the differences of the floating potentials between two poloidally or radially separated pins, respectively. One probe (*ur* – upper right) is biased to –70 V to measure the ion saturation current I_{sat}. The fifth probe is swept to record the current-voltage characteristic from which

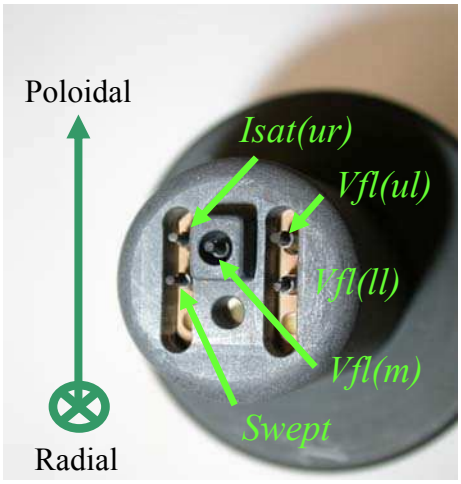

Fig. 1: Five-pin probe head used for fluctuation measurements. Three pins measure the floating potential, one probe the ion saturation current, one is swept to record the current-voltage characteristic.

the electron temperature T_e is derived. The ion density is derived from the ion saturation current.

This allows the calculation of the radial fluctuation-induced particle flux $\Gamma = \tilde{n}_i\tilde{v}_r = \tilde{n}_i\tilde{E}_\vartheta/B = \tilde{n}_i\left(\tilde{V}_{fl}(ul) - \tilde{V}_{fl}(ll)\right)/d_pB$ simultaneously with the electrostatic Reynolds stress $Re = \tilde{v}_r\tilde{v}_\vartheta \cong \tilde{E}_\vartheta\tilde{E}_r/B^2 = \left[\left(\left(\tilde{V}_{fl}(ul) - \tilde{V}_{fl}(ll)\right)/d_p\right)\left(\left(\tilde{V}_{fl}(m) - \tilde{V}_{fl}(ul)\right)/d_r\right)\right]/B^2$ where d_p and d_r are the poloidal, respectively the toroidal probe separations.

3. Experimental results

Dedicated configurations of injected power and plasma to wall distance were used in these shots with deuterium plasma. The pulses investigated are in the H-mode, and during repeated reciprocations of the probe a number of edge-localised modes (ELMs) were observable.

The probe measurements of the ELM filaments were correlated with the light emission of the D_α-line observed at the outboard divertor target (D_{out}) and that on the inboard divertor target, D_{in}. Fig. 2 shows a typical ELM between $t \cong 1.7182$ s and $t \cong 1.7210$ s (during the first reciprocation). The light emission near the outboard divertor (blue line, called "ELMa-Han outboard") and near the inboard divertor (red line, "ELMi-Han inboard") is shown on the same time scale together with the ion saturation current I_{sat} (black line). We observe a significant time delay between D_{out} and D_{in}, and likewise between D_{out} and the probe ion saturation current I_{sat}. These observations are consistent with the assumption that the ELMs are generated by a ballooning type of instability, i.e., they are born at the outboard side near the midplane as field aligned filaments with a finite extension along the magnetic field. In the scrape-off layer (SOL) they expand along magnetic field lines at a rate given by or close to the local ELM filament ion acoustic speed c_s. Their radial propagation velocity, however, is expected to be much lower, namely around 0.1 c_s or less (see e.g. [1]). The expanding filament may then be expected to first make contact with the outer divertor region since this is closest to the outboard midplane. The time delay between D_{out} and D_{in} amounts to 350 µs (see Fig. 2). For an ion acoustic speed of approximately 7×10^4 m/s (assuming $T_e \cong$

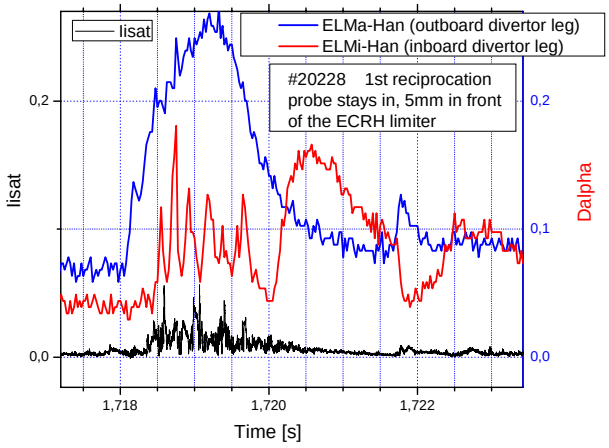

Fig. 2: Temporal evolution of the D_α-line intensity measured on the outboard divertor leg (blue line), the D_α-line intensity measured on the inboard divertor leg (red line), and of the ion saturation current measured with the probe (black line) during an ELM. Shot # 20228.

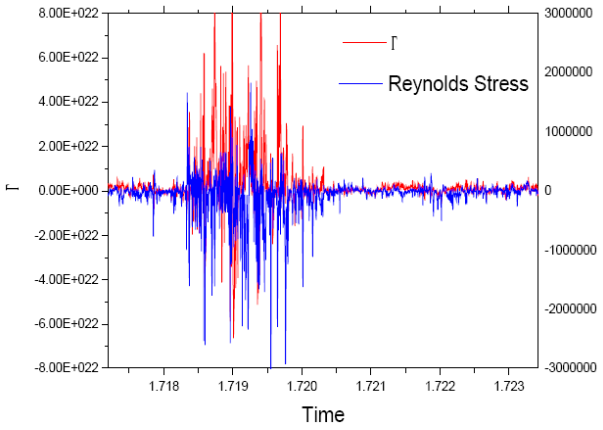

Fig. 3: Radial fluctuation-induced instantaneous flux Γ *(red line) and Reynolds stress Re (blue line) during the same shot # 20228.*

100 eV as the electron and ion temperature in the ELM filament) this corresponds to about 24 m, which is a reasonable distance, roughly corresponding to the distance along the magnetic field from the outer midplane to the inner divertor target. This observation appears to be in agreement with observations on JET by Loarte et al. [2] (see in particular their Fig. 13). We assume $T_e \cong 100$ eV since the electron temperature inside the filament reflects that one in the edge region from where the filament originates. We should stress, however, that in the SOL the electron temperature rapidly decreases due to the parallel loss of fast electrons, while the ion temperature decays much more slowly.

The time delay of about 200 μs between the signal at D_{out} and I_{sat} may be attributed to the radial propagation. For the probe in its outmost position (5 cm outside the separatrix) this would correspond to a radial velocity of about 300 m/s which equals 0.004 c_s. This is a reasonable value, taking into account the rapid decay of the electron temperature. Fig. 3 shows the particle flux and the Reynolds stress during the same shot. The cross coherence for the Reynolds stress, $\langle R_e \rangle \Big/ \sqrt{\langle v_r^2 \rangle \langle v_\vartheta^2 \rangle}$, inside the ELM, for four cumulative ELMs, is –0.55 and outside –0.31. Similarly, for the flux, we obtained 0.1, respectively 0.11. The cross coherence is stronger during ELMs which might imply a larger momentum flux.

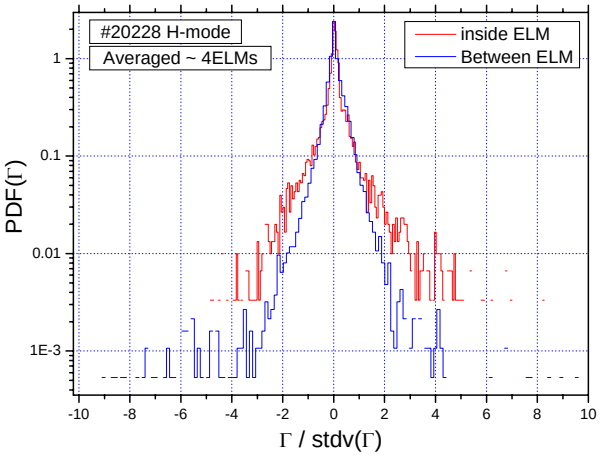

Fig. 4: Probability density function of the particle flux Γ*, once averaged over four ELMs [(red line), stdv=1.6×10[22]] and once between the ELMs [(blue line), stdv = 2.5×10[21]]. Stdv denotes the standard deviation.*

Fig. 4 shows the probability density function (PDF) of the fluctuations during ELMs (red line, showing an average over four ELMs) and in between ELMs (blue line). The PDF during ELMs has broader tails, in particular to the positive side. Thus during ELMs the transport is not only stronger but also more intermittent with larger events.

In order to examine the relation between flux and Reynolds stress we

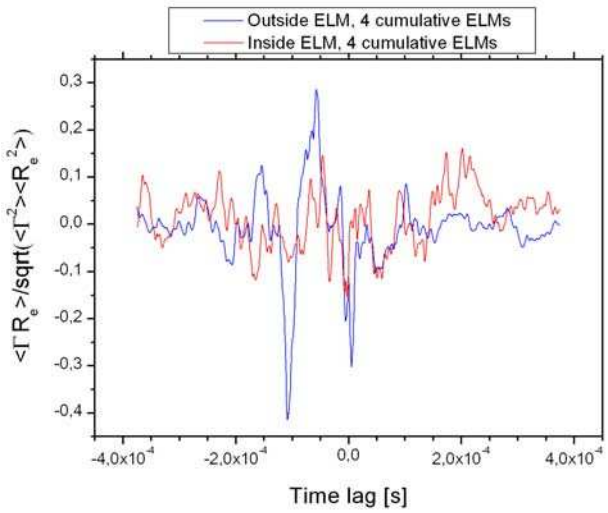

Fig. 5: Cross correlation between particle flux and Reynolds stress taken from four cumulative events, once in between ELMs (blue line) and once from ELMs (red line).

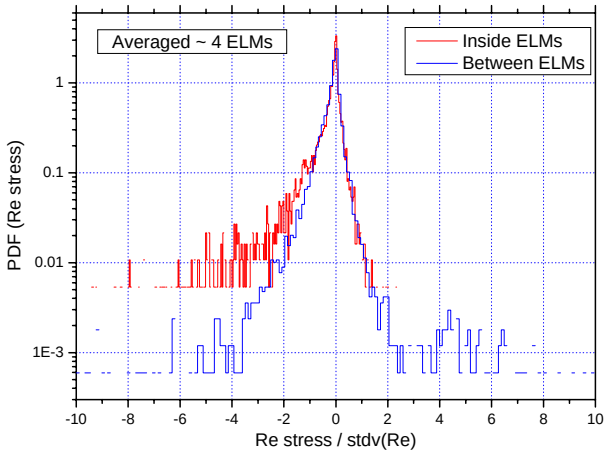

Fig. 6: Probability density function of the Reynolds stress, averaged over once in between ELMs (blue line) and once from ELMs (red line)

calculated the cross correlation ρ between these quantities, i.e., $\rho = (\Gamma R_e) \Big/ \sqrt{\langle \Gamma^2 \rangle \langle R_e^2 \rangle}$ (see Fig. 5). The figure shows a relatively big correlation both inside and outside ELMs. It seems that the correlation is better in between the ELMs (blue line) as compared to during them (red line). We note that ρ appears to be negative for zero time lag.

Fig. 6 shows the probability density function of the Reynolds stress during ELMs (red line, showing an average over four ELMs) and in between ELMs (blue line). Similar to Fig. 4, also in this case the distribution is broader for the ELM fluctuations, in particular to the negative side, which would indicate a stronger transport of momentum during ELMs than in between ELMs.

4. Conclusion

We investigated the features of transport in the SOL during ELM events and in between. We chose a particular time interval with 4 ELMs of Type I. We observe evidence for ELM filament generation near the outboard midplane whence they propagate radially outward while the filament spreads along the magnetic field lines. The transport of both density and momentum was observed to be enhanced and strongly intermittent during the ELMs, and additionally we observed a clear correlation between Γ and R_e, which, however, seems to be reduced during ELMs. It would be of utmost interest to perform similar investigations for a larger number of ELMs and also for different types of ELMs.

5. References

[1] A. Kirk et al., *Phys. Rev. Lett.* 96, 185001 (2006).
[2] A. Loarte et al., *Phys. Plasma* 11, 2668-2678 (2004).